Crack Stability in Breached Fuel

Spent Fuel and Waste Disposition

Prepared for
U.S. Department of Energy
Spent Fuel and Waste Science and Technology

Poh-Sang Lam
Robert L. Sindelar

February 8, 2021

Milestone No. M4SF-21SR010203045
SRNL-STI-2021-00056

DISCLAIMER

This information was prepared as an account of work sponsored by an agency of the U.S. Government. Neither the U.S. Government nor any agency thereof, nor any of their employees, makes any warranty, expressed or implied, or assumes any legal liability or responsibility for the accuracy, completeness, or usefulness, of any information, apparatus, product, or process disclosed, or represents that its use would not infringe privately owned rights. References herein to any specific commercial product, process, or service by trade name, trade mark, manufacturer, or otherwise, does not necessarily constitute or imply its endorsement, recommendation, or favoring by the U.S. Government or any agency thereof. The views and opinions of authors expressed herein do not necessarily state or reflect those of the U.S. Government or any agency thereof.

Prepared by
Savannah River National Laboratory
Savannah River Nuclear Solutions
Aiken, South Carolina 29808

Savannah River National Laboratory is a multiprogram laboratory managed and operated by Savannah River Nuclear Solutions, LLC, for the U.S. Department of Energy under contract DE-AC09-09SR22505.

EXECUTIVE SUMMARY

This report describes the fracture mechanics formalism to evaluate the stability of cracks in a fuel cladding. Recognized consensus-body linear elastic fracture mechanics (LEFM) was applied to identify the crack instability length, or the length at which unstable mechanical crack extension would occur, as a function of pellet swelling loading (radial strain and fraction conversion from UO_2 to U_3O_8) at the local cracked cladding region for two postulated fracture toughness (K_{IC}) values of the cladding. The crack opening displacement (COD) and the crack opening area (COA) were also identified. This analysis informs evaluations for crack extension and the potential for pellet debris loss from the fuel rod for cases of pellet oxidation in dry storage canisters where inadvertent residual water may undergo radiolysis causing oxidizing conditions to pellets exposed to the canister environment through breached cladding.

The Timoshenko solution [8] was first used to estimate the press-set pressure exerted by the oxidized pellet on the cladding. Based on the pressure, the stress in the cladding was obtained from the classic solution of a pressurized cylindrical structure; and the strain was calculated from linear elasticity (Hooke's law). This approach inevitable leads to a very high stress state far exceeding the elastic limit of the cladding material. Therefore, the subsequent LEFM analysis results in a conservative (short) critical crack length with a corresponding critical crack opening area/displacement. For example, at the onset of oxidized pellet-cladding interaction (OPCI) when the UO_2 to U_3O_8 conversion fraction is 0.4 [4 Table 3-6], the critical crack length is estimated as 30 μm for K_{IC} = 25 MPa√m and is 330 μm for K_{IC} =90 MPa√m, and the corresponding crack opening displacements are 2 μm and 27 μm, respectively. It is emphasized that the extent of growth from an unstable crack to a stable crack is limited by the extent of additional pellet oxidation along the length of the rod. In other words, continued crack extension beyond only a local region of pellet oxidization would not occur due to removal of the displacement-based loading condition. Additional improvements for evaluation of flaw tolerance under pellet swelling loading are suggested. Additional characterization of the fracture toughness of High-Burnup (HBU) cladding is also suggested.

This report fulfills the M4 milestone M4SF-21SR010203045, "Crack Opening in Breached Fuel" under Work Package Number SF-21SR01020304.

TABLE OF CONTENTS

LIST OF FIGURES

LIST OF TABLES

ACRONYMS

COA	Crack opening area
COD	Crack opening displacement
DOE	U.S. Department of Energy
HBU	High Burn-Up
LEFM	Linear Elastic Fracture Mechanics
LWR	Light Water Reactor
NE	Nuclear Energy
NEUP	Nuclear Energy University Program
NRC	Nuclear Regulatory Commission
OD	Outer diameter
OPCI	Oxidized Pellet-Cladding Interaction
PWR	Pressurized Water Reactor
PNNL	Pacific Northwest National Laboratory
RH	Relative Humidity
SFWD	Spent Fuel and Waste Disposition
SINTAP	Structural INTegrity Assessment Procedures
SNF	Spent Nuclear Fuel
SNL	Sandia National Laboratories
SNTT	Spiral Notch Torsion Test
SRNL	Savannah River National Laboratory

ACKNOWLEDGMENTS

The authors gratefully acknowledge the support of Ned Larson, U.S. Department of Energy, Office of Nuclear Energy, Office of Spent Fuel and Waste Disposition, Office of Spent Fuel & Waste Science and Technology, for his office's sponsorship of this work, and supported by Control Account Manager Sylvia Saltzstein from Sandia National Laboratories and deputy CAM Brady Hanson from the Pacific Northwest National Laboratory.

1. INTRODUCTION

The experiments conducted by Einziger and Cook (1985) [1], Einziger and Strain (1986) [2], and Novak and Hastings (1984) [3] have demonstrated that pellet oxidation caused by small cladding defects could breach the fuel rod under dry storage of the spent nuclear fuel (SNF). In the process of pellet oxidation, the uranium dioxide (UO_2) may convert to triuranium octoxide (U_3O_8). As the uranium oxide experiences this transformation, its density changes from 10.96 g/cm^3 to 8.35 g/cm^3, which leads to pellet volume expansion, and these affected pellets would be in contact with cladding inner diameter. The oxidizing pellets may continue to swell and could eventually exert sufficient stress on the cladding to initiate crack propagation from the original defect. This action could split the fuel rod axially.

This report focuses on the evaluation of the cladding stress and fracture due to pellet expansion following the analysis results given by Shukla, Sindelar, and Lam (2019) [4] on pellet volume and diametrical changes as UO_2 converts to U_3O_8. The kinetics of uranium oxide transformation and the burnup dependence [5], the fracture of pellets [6], and the external rim on pellets [7] are not considered here.

Timoshenko solutions [8] are used to estimate the press-fit pressure exerted by the pellet due to volume/diametrical increase against the cladding. For generality, thick-wall cylinder solutions and Hooke's law are used to calculate the stresses and strains on the cladding based on the press-fit pressure. The details can be found in Section 2. It follows in Section 3 that the cladding hoop stress is input to API 579-1/ASME FFS-1 Fitness-For-Service code [9] for calculating stress intensity factor (K) for a length $2c$ of through-wall crack in a fuel rod cladding. The critical crack length and critical crack opening area (COA) can be obtained by comparing the calculated K to the cladding fracture toughness K_{IC}. Two values of K_{IC} (25 and 90 MPa$\sqrt{}$m) are selected in the calculation to cover the possible range of the material property. The crack length corresponding to the condition $K = K_{IC}$ is defined as the critical crack length, from which the critical crack opening area and the critical crack opening displacement can be calculated. Lastly, the results and path forward are discussed in Section 4. Appendix A is provided for alternative methods to calculate K and COA. It can be seen that the API 579 procedure would provide the most conservative results.

The extent of crack extension from an unstable crack at the critical crack length to a stable crack, and similarly the extent of crack opening area, and crack opening displacement are limited by the extent of additional pellet oxidation along the length of the rod. In other words, crack extension beyond a local region of pellet oxidization would not occur due to removal of the applied displacement-based loading condition. The extent of pellet oxidation up the fuel rod is beyond the scope of this report. No evaluation is attempted for loss of pellet fragments from an opened crack, or for the relief on cladding press-fit pressure due to loss of pellet fragments.

2. STRESS ANALYSIS OF OXIDIZED PELLET-CLADDING INTERACTION (OPCI)

This section describes a linear elastic approach to calculate cladding failure stress and deformation as a result of the oxidized pellet-cladding interaction (OPCI), and to estimate the critical crack length, crack opening area, and opening displacement based on the principle of Linear Elastic Fracture Mechanics (LEFM) and a set of bounding cladding fracture toughness (K_{IC}).

Typical light water reactor fuel rod and pellet dimensions are used in this analysis: fuel rod (or cladding) outer diameter (OD) is 10.92 mm; pellet diameter is 9.36 mm; and the cladding thickness is 0.6 mm.

2.1 General Solution for a Pressurized Cylinder

The cladding is a relatively thin shell structure with $R_i/t = 8.1$, where R_i is the inner radius of the fuel rod (or cladding) and t is the cladding wall thickness). For generality purposes, the stress solution for thick-wall cylinder is presented below and will be used throughout this report.

For a cylinder with outside radius R_o and inner radius R_i subjected to internal pressure p_i and external pressure p_o, Timoshenko [8] showed that

$$\sigma_h = \frac{p_i R_i^2 - p_o R_o^2 + (p_i - p_o) R_i^2 R_o^2 / r^2}{R_o^2 - R_i^2} \quad (1)$$

$$\sigma_r = \frac{p_i R_i^2 - p_o R_o^2 - (p_i - p_o) R_i^2 R_o^2 / r^2}{R_o^2 - R_i^2} \quad (2)$$

where σ_h is the circumferential or hoop stress at a radial distance r from the center of the cylinder, σ_r is the radial stress, and the axial stress is not considered in the present case. As expected, Eq. (2) suggests that $\sigma_r = 0$ on unpressurized surface of the cylinder and $\sigma_r = -p$ on pressurized surface.

2.2 Press fit Solution for Oxidized Pellet-Cladding Interaction (OPCI)

Figure 1 shows that two cylinders are press-fitted against each other at $r = R$ with a radial interference δ_R. The outer cylinder has material properties Young's modulus (E_o) and Poisson's ratio (ν_o). For the inner cylinder, these material properties are denoted as E_i and ν_i.

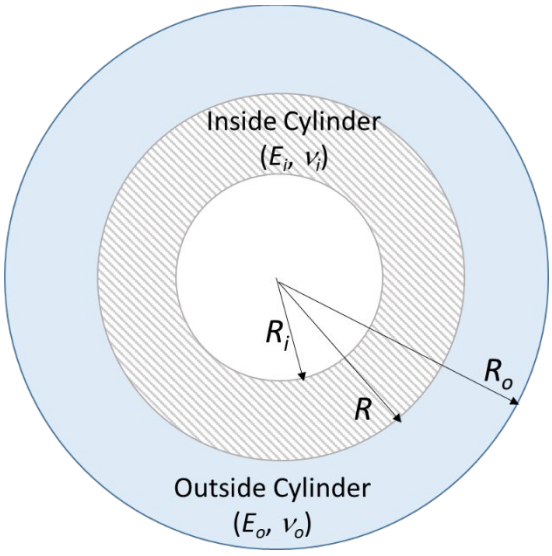

Figure 1. Press fit of two cylinders

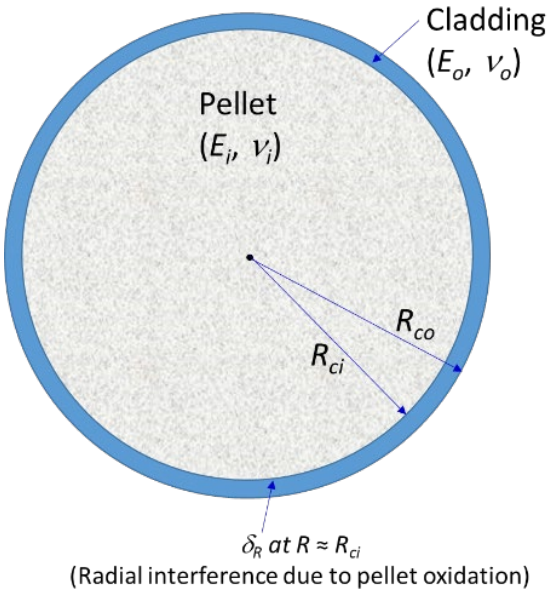

Figure 2. Oxidizing pellet stresses the cladding (not to scale)

2.2.1 Cladding Stresses

The Interface pressure (or press-fit pressure), p, can be expressed as [8]

$$p = \frac{\delta_R}{\frac{R}{E_o}\left(\frac{R_o^2+R^2}{R_o^2-R^2}+\nu_o\right)+\frac{R}{E_i}\left(\frac{R^2+R_i^2}{R^2-R_i^2}-\nu_i\right)} \quad (3)$$

In the case of OPCI (see Fig. 2), the following parameters are used in Eq. (3): $R = R_{ci}$, which is the cladding inner radius; $R_o = R_{co}$, which is the cladding or fuel rod outer radius; $R_i = 0$ (solid pellet); δ_R is the radial growth of the pellet due to oxidation, E_o is the Young's modulus of the cladding, ν_o is the Poisson's ratio of the cladding, E_i is the Young's modulus of the pellet, and ν_i is the Poisson's ratio of the pellet. The resulting expressions for the cladding stresses are

Hoop (or circumferential) stress at the cladding inner diameter: $\sigma_{ch} = p\frac{R_{co}^2+R_{ci}^2}{R_{co}^2-R_{ci}^2}$ (4)

Radial stress at the cladding inner diameter: $\sigma_{cr} = -p$ (5)

Hoop stress at the cladding outer diameter: $\sigma_{oh} = \frac{2p}{R_{co}^2-R_{ci}^2}$ (6)

Radial stress at the cladding outer diameter: $\sigma_{or} = 0$ (7)

Note that σ_{ch} (Eq. (4)) is always greater than σ_{oh} (Eq. (6)). For conservatism, the cladding hoop stress σ_{ch} at the inner diameter of the cladding is used for the fracture mechanics calculation in Section 3. Also note that both Eqs. (4) and (6) can be reduced to pr_m/t for thin shell structures, where r_m is the mean radius of the cladding and t is the cladding wall thickness.

The stresses for the pellet are nor relevant in the present case, and therefore they are not calculated here. Nevertheless, it is interesting to note that the pellet hoop and radial stresses on the interface are both equal to the negative OPCI pressure (p).

2.2.2 Cladding Strains

On the cladding inner surface, a biaxial stress state exits because the axial loading of the fuel rod is not considered in the present case. By Hooke's law, the hoop (circumferential) strain ε_h is obtained as

$$\varepsilon_h = (\sigma_{ch} - \upsilon_0\sigma_{cr})/E_o = (\sigma_{ch} + \upsilon_0 p)/E_o \quad (8)$$

In the case of uniform radial expansion, the hoop strain (ε_r) and radial strain (ε_r) are the same:

$$\varepsilon_h = \varepsilon_r \quad (9)$$

The radial strain of the cladding is sometimes denoted as ($\Delta R/R$), where R represents the radius and ΔR is the increase of radius.

2.2.3 Young's Modulus of the Oxidizing Pellet (Ei)

In the calculation for press-fit pressure (p) with Eq. (3), the Young's modulus of the pellet (E_i) is needed. During the oxidation process, a series of conversion from UO_2 to U_3O_8 is taking place [e.g. 1-7].

Therefore, for different stage of the uranium oxide, the corresponding Young's modulus must be known for the calculation. The "rule of mixtures" developed for composite materials is adopted here:

$$E_i = E_{UO2}V_{UO2} + E_{U3O8}V_{U3O8} \quad (10)$$

where E_{UO2} and E_{U3O8} are the Young's moduli of UO_2 and U_3O_8, respectively; and V_{UO2} and V_{U3O8} are their volume fractions in the mixture (oxidizing pellet) with the condition that $V_{UO2} + V_{U3O8} = 1$. The volume fractions in this analysis are approximated by the Conversion Fraction reported in Shukla, Sindelar, and Lam [4, Table 3-6].

The Young's modulus was given by Jiang and Wang [10] in their dynamic analysis of SNF system during transportation:

$$E_{UO2} = 201.3\ GPa \quad (11)$$

In a thin film experiment conducted by Lin et al. [11], different uranium oxide phases were obtained by controlling the oxygen in the total gas flow rate (f_{O2}) in the chamber. The Young's moduli for the cubic UO_2 film (f_{O2} = 10%) and for the U_3O_8 thin films (f_{O2} > 15%) were reported as 195 and 147 GPa, respectively. To be consistent with SNF analysis at Oak Ridge National Laboratory [10], the Young's modulus of U_3O_8 in the present work is estimated by scaling Eq (11) with the thin film results:

$$E_{U3O8} = E_{UO2} \times \frac{147\ GPa}{195\ GPa} = 151.8\ GPa \quad (12)$$

The volume fractions of UO_2 (V_{UO2}) in Eq. (10) are approximated by the Conversion Fractions reported by Shukla, Sindelar, and Lam [4, Table 3-6]. It should be noted that $V_{U3O8} = 1 - V_{UO2}$.

The Poisson's ratio of the pellet is not adjusted with the change of volume fraction, and $\nu_i = 0.32$ [10] is used throughout the calculation.

2.2.4 Cladding Stress Calculation Results

The analysis parameters were selected from the previous report [4]:

(1) Cladding

Outer radius (fuel rod radius): R_{co}= 5.46 mm

Inner radius: R_{ci}= 4.86 mm

Cladding wall thickness: t= 0.6 mm

Young's modulus: E_o = 100 GPa (typical for high burn-up fuel)

Poisson's ration: ν_i= 0.37

(2) Pellet

Radius= 4.68 mm

Young's modulus of UO_2: E_{UO2} = 201.3 GPa

Young's modulus of U_3O_8: E_{U3O8}= 151.8 GPa

Young's modulus of pellet: Use the rule of mixtures, Eq. (10)

Poisson's ration ν_o= 0.32

(3) Pellet-Cladding Interface

Radial growth of the pellet due to oxidation: δ_R [4, Table 3-6]

Figure 3 shows the calculated OPCI pressure (press-fit) using Eq. (3) and the cladding hoop stress using Eq. (4). They are plotted as functions of the conversion fraction from UO_2 to U_3O_8 reported in Shukla, Sindelar, and Lam [4, Table 3-6]. For additional information, the diameter change of the oxidized pellet [4, Table 3-6] is also plotted. The cladding hoop stress is the main input to calculate the stress intensity factor (K or K_I) and crack opening area (COA).

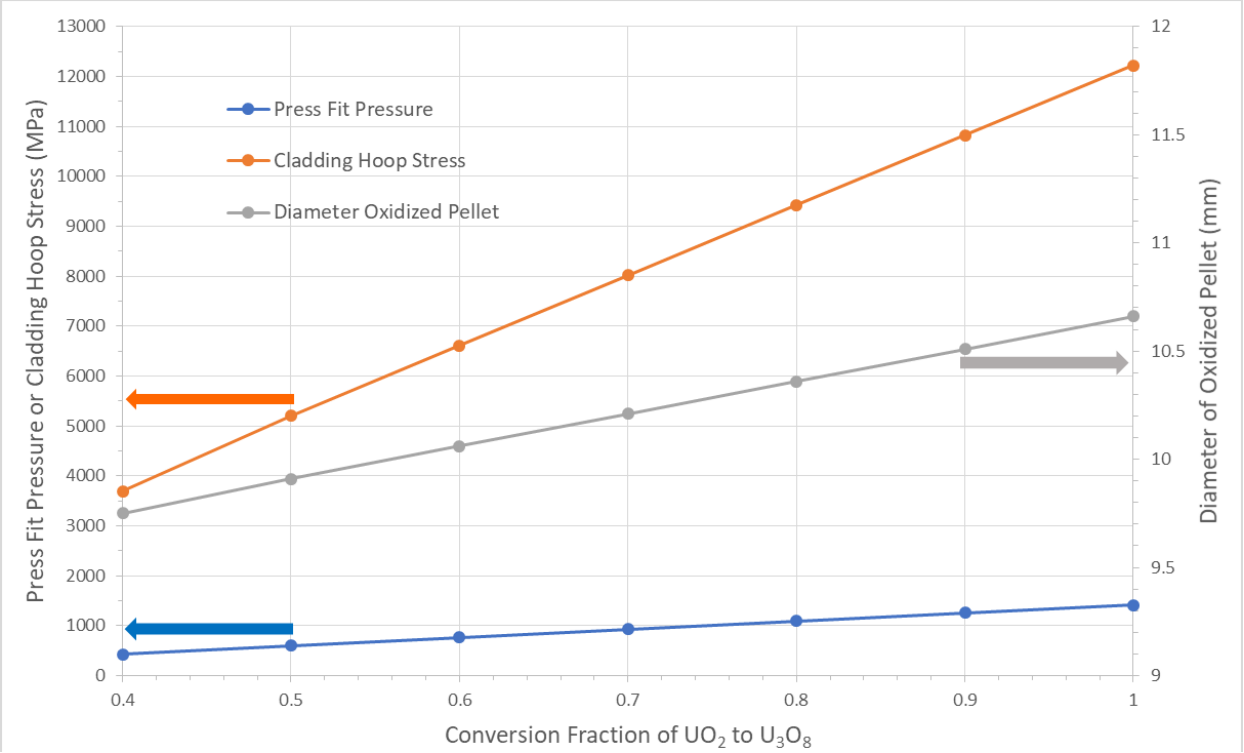

Figure 3. Cladding hoop stress and OPCI pressure vs. pellet UO_2 to U_3O_8 conversion fraction

3. FRACTURE ANALYSIS

It was reported previously that, for UO_2 to U_3O_8 conversion fraction less than 0.4, the oxidized pellets are not in contact with the cladding, and cladding breach due to pellet volume expansion will not occur [4]. Therefore, fracture analysis is performed in this section to determine the critical crack length, crack opening area (COA), and crack opening displacement (COD) only for conversion fraction greater and equal to 0.4.

Based on LEFM, stress intensity factor (K) calculated from the applied load (in the present case, the cladding hoop stress) is compared to the fracture toughness (K_{IC}) of the cladding material. For a given hoop stress (calculated in Section 2), the crack length corresponds to $K = K_{IC}$ is defined as the critical crack length. This critical crack length is then used to calculate the critical COA.

3.1 Determination of Critical Crack Length

API 579 (2016) Annex 9B [9] is used to calculate the stress intensity factors at the crack tips of an axial through-wall crack in a cylinder (Fig. 4). Other stress intensity factor solutions [e.g., 12-17] can also be used, but API 579 appears to provide more conservative results, as documented in Appendix A.

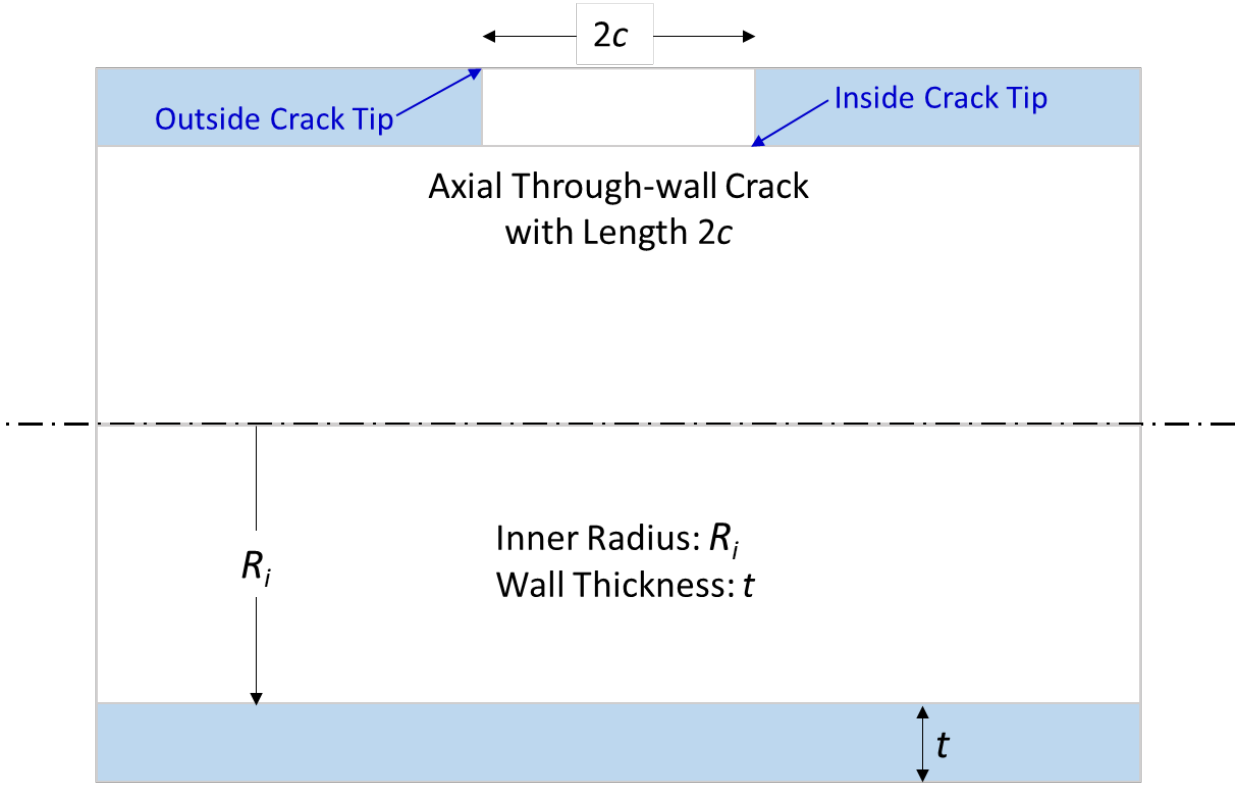

Figure 4. Sketch of an axial through-wall crack in a cylinder

In the API 579 formulation [9, Annex 9B], for a crack illustrated in Figure 4 is loaded with a membrane stress (σ_m) without bending, the stress intensity factor is

$$K_I = \sigma_m G_0 \sqrt{\pi c} \tag{13}$$

where G_0 is the influence coefficient and is expressed as

$$G_0 = \frac{A_0 + A_1\lambda + A_2\lambda^2 + A_3\lambda^3}{1 + A_4\lambda + A_5\lambda^2 + A_6\lambda^3} \tag{14}$$

and

$$\lambda = \frac{1.818c}{R_i t} \quad (15)$$

For the fuel rod with the dimensions specified in Section 2.2.4 (R_{ci}= 4.86 mm), the wall thickness to inner radius ratio *t/Ri* is 0.1235. The constants A_i (*i*=1 to 6) can be obtained from API 579 and are listed in Table 1.

Table 1. Constants for Calculating Influence Coefficient G_0 for Evaluating Stress Intensity Factor

Crack Tip Location	For *t/Ri* = 0.1235 (by interpolation [9, Tables 9B.6 and 9B.7]) (Cladding Wall Thickness *t* = 0.6 mm and Fuel Inside Radius *Ri* = 4.86 mm)						
	A_0	A_1	A_2	A_3	A_4	A_5	A_6
Outside Surface	0.99487	0.52801	0.19149	0.00000	0.18334	0.03177	0.00015
Inside Surface	1.00766	0.13948	0.23996	0.00000	0.25820	0.01009	-0.00025

The fracture toughness (K_{IC}) of the cladding material must be known for the determination of the critical crack length. By reviewing the open literature, two K_{IC} values (25 and 90 MPa√m) [e.g. 18, 19] are used to bound the analysis results. The critical crack length is plotted as a function of UO_2 to U_3O_8 conversion fraction is shown in Figure 5. The corresponding cladding hook strains (Eq. (8)) can be seen as the secondary x-axis on the top of the figure.

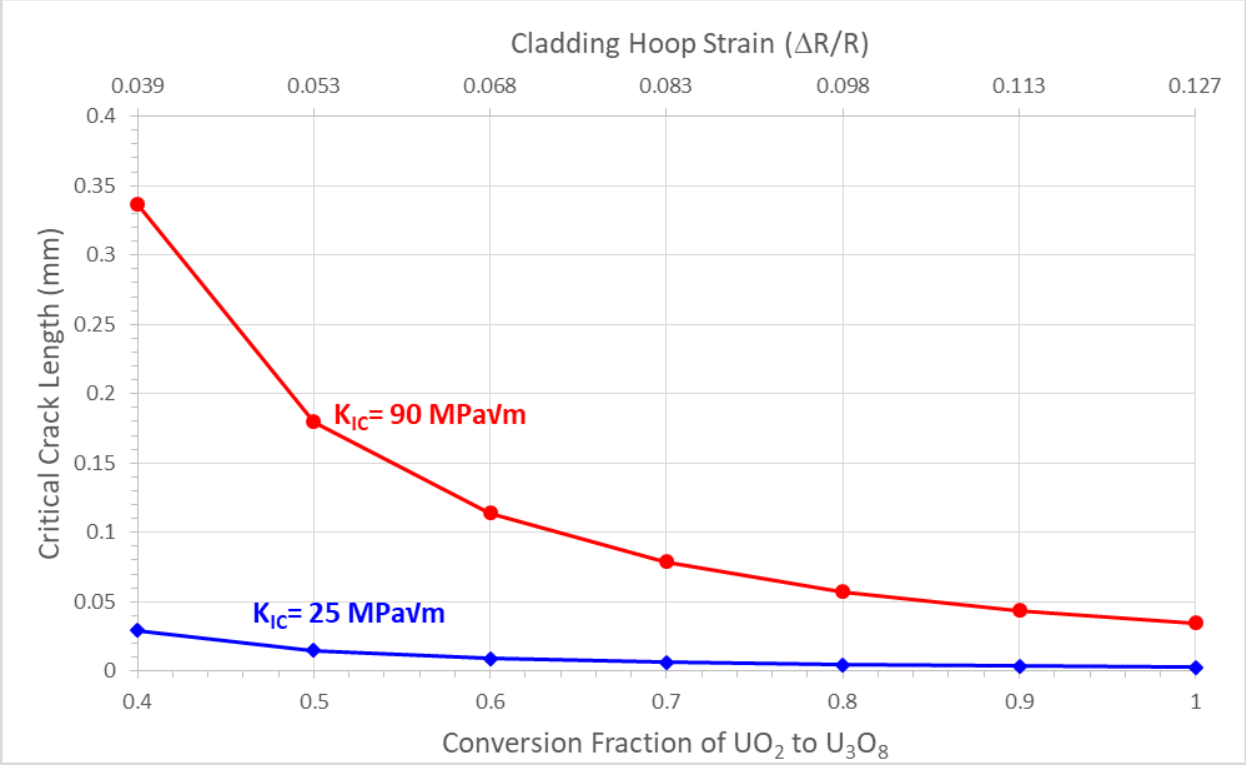

Figure 5. Critical crack length vs. conversion fraction of uranium oxides and the cladding hoop strain

3.2 Determination of Critical Crack Opening Area and Crack Opening Displacement

API 579 also provides the formula to calculate COA [9, Annex 9E]:

$$COA = \sigma_m H_0 \frac{2\pi c^2}{E} \tag{16}$$

where E is the Young's modulus of the material and H_0 is the influence coefficient and is defined as

$$H_0 = \frac{A_0+A_1\lambda+A_2\lambda^2+A_3\lambda^3}{1+A_4\lambda+A_5\lambda^2+A_6\lambda^3+A_7\lambda^4} \tag{17}$$

Table 2 lists the constants A_i (i=0 to 7) for calculating COA with Eq. (16) and λ has been defined in Eq. 15.

Table 2. Constants for Calculating Influence Coefficient H_0 for Evaluating Crack Opening Area

Crack Tip Location	For Ri/t = 8.1 (by interpolation [9, Tables 9E.1 and 9E.2]) (Fuel Inside Radius Ri = 4.86 mm and Cladding Thickness t = 0.6 mm)							
	A_0	A_1	A_2	A_3	A_4	A_5	A_6	A_7
Outside Surface	1.00755	0.46495	0.40483	0.34536	0.07032	0.54307	-0.04790	0.00179
Inside Surface	1.00861	-0.11732	0.22262	0.00000	0.05803	0.00356	-0.00020	0.00000

Note that the Young's modulus is needed to evaluate COA. In the present case, it is the Young's modulus of the cladding, which has been given in Section 2.2.4 (E_o = 100 GPa).

An approximate and convenient method to estimate the crack opening displacement is to assume that the deformed crack takes the form of an ellipse [e.g., 4, 17, 20]. Therefore, crack opening displacement (COD) can be calculated by equating COA (Eq. (16)) to the area of an ellipse πbc, where the equivalent crack opening displacement ($2b$) is the minor axis of this ellipse and its major axis 2c is the axial crack length (Fig. 4). Therefore,

$$COD = 2b = 4cH_0 \frac{\sigma_m}{E} \tag{18}$$

The calculated critical COA and COD are presented in Figures 6 and 7 as functions of conversion fraction from UO_2 to U_3O_8. As in Figure 5, the corresponding cladding hoop strain can be read from the secondary x-axis on the top of the figure.

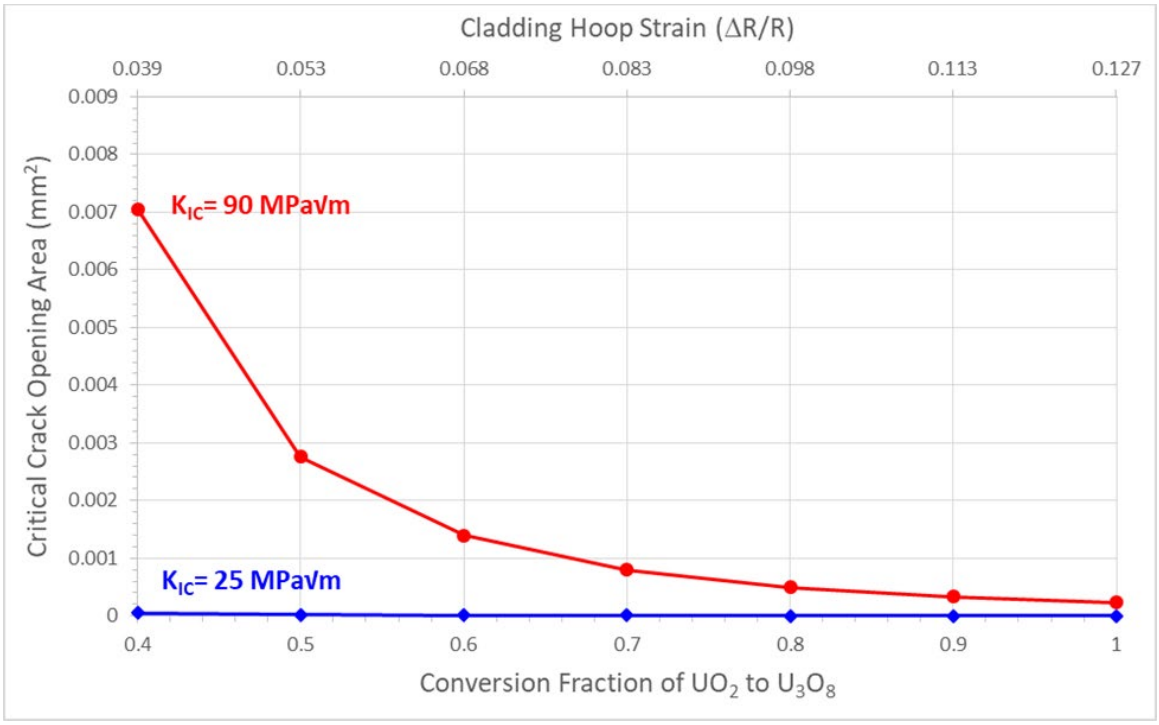

Figure 6. Critical crack opening area vs. conversion fraction of uranium oxides and the cladding hoop strain

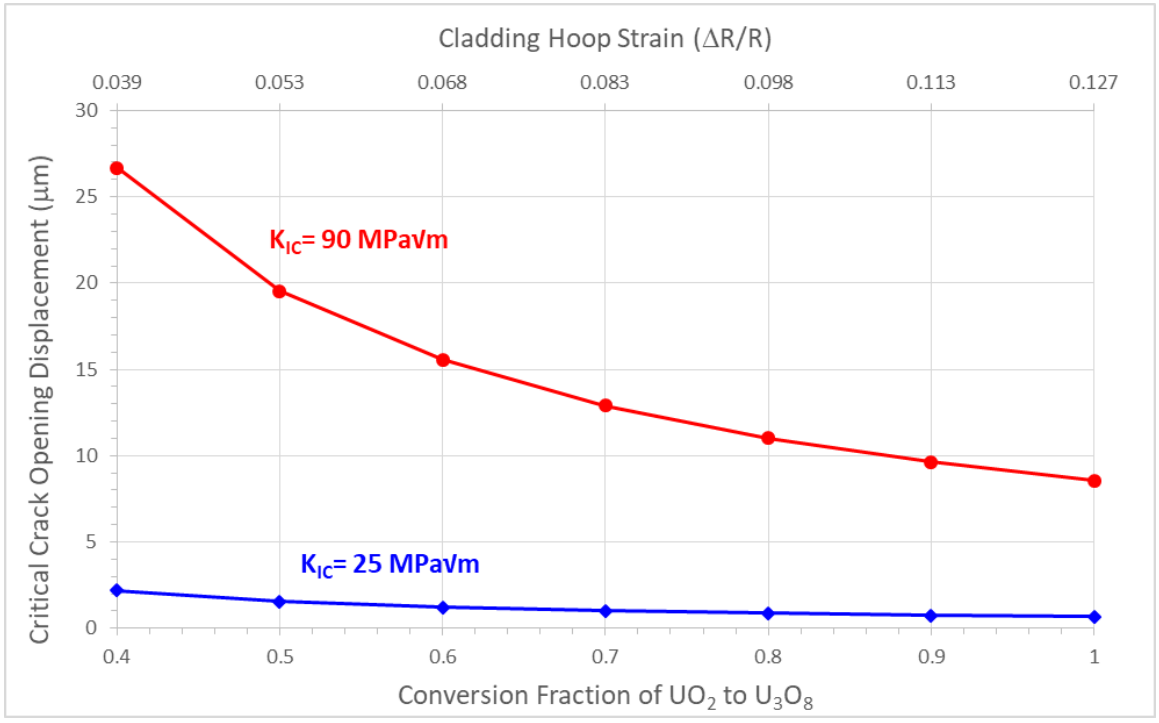

Figure 7. Critical crack opening displacement vs. conversion fraction of uranium oxides and the cladding hoop strain

4. CONCLUDING REMARKS

In the present work, Timoshenko solution [8] was first used to estimate the press-set pressure exerted by the oxidized pellet on the cladding. Based on the pressure, the stress in the cladding is obtained from the classic solution of a pressurized cylindrical structure; and the strain is calculated from linear elasticity (Hooke's law). This approach inevitable leads to a very high stress state far exceeding the elastic limit of the cladding material. Therefore, the subsequent LEFM analysis results in a conservative (short) critical crack length with a corresponding critical crack opening area/displacement. For example, at the onset of OPCI when the UO_2 to U_3O_8 conversion fraction is 0.4 [4 Table 3-6], the critical crack length is estimated as 30 μm for K_{IC} = 25 MPa√m and is 330 μm for K_{IC} =90 MPa√m, and the corresponding crack opening displacements are 2 μm and 27 μm, respectively. Of course, the true value of K_{IC} is to be determined, but the updated prediction should fall within those limiting values. If the restriction needs to be relaxed, then elastic-plastic finite element analysis is recommended. On the other hand, the sizes of the original artificial defects in the SNF experiment by Einziger and Strain (1986) [2] ranged from 8 to 760 μm, which seem to be comparable to the present calculation results. Therefore, the small crack sizes as predicted from the present work could initiate crack propagation and extend an initial breach in the fuel rod through pellet oxidation. Note that the smallest defect size (8 mm) in the experiment of Einziger and Strain was used to approximate the size of a stress corrosion cracking-type cladding breach [2].

The fracture toughness (K_{IC}) is an important parameter to predict cladding failure. It is considered as a material property and must be determined experimentally. Work has been done in this area for decades [e.g. 21], but due to the complexity in zirconium alloy composition, irradiation history and environments, hydride orientation [22, 23], and test methods, etc., a more structured approach may be needed, as pointed out in the white paper by Sindelar, Louthan, and Hanson (2016) [24].

The fracture toughness of high burnup cladding has not been fully characterized. The testing may require more considerations that include the radioactivity and material availability. Nontraditional test methods, such as the hot cell-ready, small specimen-oriented Spiral Notch Torsion Test (SNTT) developed at Oak Ridge National Laboratory [25, 26], may be one of the options. The companion advanced fracture mechanics and numerical methods may also need to be further developed to account for the unusual specimen shape and size in order to extract useful fracture parameters in consistent with the ASTM standard requirements.

5. REFERENCES

[1] R. E. Einziger, and J.A. Cook, "Behavior of Breached Light Water Reactor Spent Fuel Rods in Air and Inert Atmospheres at 229 °C," Nuclear Technology, Vol. 69. pp. 55–71, 1985.

[2] R. E. Einziger and R. V. Strain, "Behavior of Breached Pressurized Water Reactor Spent-Fuel Rods in an Air Atmosphere between 250 and 360 °C," Nuclear Technology, Vol. 75. pp. 82–95, 1986.

[3] J. Novak and I. J. Hastings, "Post-Irradiation Behavior of Defected UO_2 Fuel Elements in Air at 220-250 °C," Proc. NRC Workshop in Spent Fuel/Cladding Reaction During Dry Storage, Gaithersburg, Maryland, August 17-18, 1983, NUREG/CR-0049, D. Reisenweaver, Ed., U.S. Nuclear Regulatory Commission, 1984.

[4] P. Shukla, R. Sindelar, and P. S Lam, *Consequence Analysis of Residual Water in a Storage Canister – Preliminary Report*, Milestone No. M2SF-19SR010201055 (SRNL-STI-2019-00495), September 2019, Savannah River National Laboratory, Aiken, South Carolina, USA.

[5] B. D. Hanson, *The Burnup Dependence of Light Water Reactor Spent Fuel Oxidation*, PNL–11929. Pacific Northwest National Laboratory, Richland, WA, 1998.

[6] T. M. Ahn, *Dry Oxidation and Fracture of LWR Spent Fuels*, NUREG–1565, ML040150720. U. S. Nuclear Regulatory Commission, Washington, DC, 1996.

[7] L. E. Thomas, O. D. Slagle, and R. E. Einziger, "Nonuniform Oxidation of LWR Spent Fuel," Journal of Nuclear Materials, 184, pp. 117-126, 1991.

[8] S. P. Timoshenko, *Strength of Materials, Part II, Advanced Theory and Problems*, D Van Nostrand Co., Inc., Princeton, New Jersey, 1st Ed. 1930; 2nd Ed., 1941; 3rd Ed., 1956.

[9] API 579-1/ASME FFS-1, Fitness-For-Service, American Petroleum Institute, Washington, DC., USA, June 2016.

[10] H. Jiang and J.-A. Wang, "Spent nuclear fuel system dynamic stability under normal conditions of transportation," Nuclear Engineering and Design, 310, (2016), pp. 1–14.

[11] J. Lin, I. Dahanb, B. Valderramac, and M. V. Manuelc, "Structure and properties of uranium oxide thin films deposited bypulsed dc magnetron sputtering," Applied Surface Science, 301 (2014), pp. 475–480.

[12] H. Tada, P. C. Paris and G. R. Irwin, *The Stress Analysis of Cracks Handbook, Second Edition*, Paris Productions Incorporated (and Del. Research Corporation), Saint Louis, Missouri, 1985.

[13] S. Al Laham, *Stress Intensity Factor and Limit Load Handbook*, SINTAP Report, Sub-Task 2.6, Nuclear Electric Report EPD/GEN/REP/0316/98, British Energy Generation Ltd, UK, pp. 1998.

[14] SINTAP: Structural INTegrity Assessment Procedures for European Industry. Final Revision, EU Project BE 95-1462, Brite Euram Programme, 1999

[15] BS 7910:2013 + A1: 2015 - *Guide to methods for assessing the acceptability of flaws in metallic structures*, British Standards Institution (BSI), London, UK, 2015.

[16] R. Bourga, B. Wang, P. Moore, and Y. J. Janin, "Comparison of BS 7910 and API 579-1/ASME FFS-1 solutions with regards to leak-before-break," Paper No. PVP2016-63876, Proceedings of the ASME Pressure Vessels & Piping Conference, Vancouver, BC, Canada, July 2016.

[17] P. J. Gill, *Investigating Leak Rates for "Leak-Before-Break" Assessment*, PhD Dissertation, The University of Manchester, Manchester, UK, 2013.

[18] P. A. Raynaud, D. A. Koss, A. T. Motta, and K. S. Chan, "Fracture Toughness of Hydrided Zircaloy-4 Sheet Under Through-Thickness Crack Growth Conditions," Journal of ASTM International, Vol. 5, No. 1, Paper ID JAI101183, pp. 1-15, 2007.

[19] R. L. Sindelar, A. J. Duncan, M. E. Dupont, P. S. Lam, M. R. Louthan, Jr., and T. E. Skidmore, *Materials Aging Issues and Aging Management for Extended Storage and Transportation of Spent Nuclear Fuel*, NUREG/CR-7116 (SRNL-STI-2011-00005), Prepared for the Division of Storage and Transportation, Office of Nuclear Reactor Regulation, U.S. Nuclear Regulatory Commission, Washington, DC, November 2011.

[20] Chu, S., Flaw Growth and Flaw Tolerance Assessment for Dry Cask Storage Canisters, No. 3002002785, Electric Power Research Institute, Palo Alto, CA., USA, 2014.

[21] A. Machiels, *Fracture Toughness Data for Zirconium Alloys: Application to Spent Fuel Cladding in Dry Storage*, Electric Power Research Institute, Palo Alto, CA, 1001281, 2001.

[22] M. C. Billone, T. A. Burtseva, and R. E. Einziger, “Ductile-to-brittle transition temperature for high-burnup cladding alloys exposed to simulated drying-storage conditions,” Journal of Nuclear Materials, 433, pp. 431-448, 2013.

[23] R. L. Kesterson, P. S. Korinko, P. S. Lam, and R. L. Sindelar, “Hydride Effects on Discharged Fuel Clad Related to Accident Conditions During Dry Storage and Handling,”, in *Zirconium in the Nuclear Industry: 18th International Symposium*, ASTM STP1597, R. J. Comstock and A. T. Motta, Eds., ASTM International, West Conshohocken, PA, pp. 1192–1223, 2018.

[24] R. L. Sindelar, M. R. Louthan, Jr., and B. D. Hanson, *White Paper Summary of 2nd ASTM International Workshop on Hydrides in Zirconium Alloy Cladding, Jackson, WY, June 2014*, FCRD-UFD-2015-000533 (SRNL-STI-2015-00256), U.S. Department of Energy, May 29, 2015.

[25] J. A. Wang, "Fracture Toughness Evaluation for Spent Nuclear Fuel Clad Systems Using Spiral Notch Torsion Fracture Toughness Test," ORNL/TM-2019/1204, Oak Ridge National Laboratory, Oak Ridge, Tennessee, USA, June 2019.

[26] J. A. Wang, "Fracture toughness evaluation for Zr-4 clad tubing structure with pellet inserts," Theoretical and Applied Fracture Mechanics, 108 (2020) 102657

APPENDIX A: EVALUATION OF STRESS INTENSITY FACTOR CALCULATIONS

This page intentionally left blank.

APPENDIX A

Stress intensity factors and other fracture parameters can be calculated with many handbook and international consensus code solutions [e.g., 9, 14, 15]. In this appendix, the results from Tada, Paris, and Irwin [12] and from European structural integrity assessment procedure (SINTAP) [13, 14] are compared with API 579 [9] used in the main body of this report.

Only the case relevant to this report is investigated, that is, an axial through-wall crack in the fuel rod cladding subject to volume expansion of the fuel pellets due to oxidation that UO_2 is converted to U_3O_8.

The cladding deformation can be approximated by an axisymmetric condition. Under this simplification, the cladding hoop strain (ε_h) is expressed as (see Section 2):

$$\varepsilon_h = \Delta R/R$$

where R is the cladding mean radius and ΔR is the amount of cladding expansion. Instead of using a full field elastic solution (such as Eq. 8* in Section 2). A simple, uniaxial Hooke's law is used to calculate the hoop stress (σ_h) in the cladding with the Young's modulus E:

$$\sigma_h = E\varepsilon_h$$

The hoop stress (σ_h) is the main input to fracture analysis. Figure 4 shows the crack configuration. The formulations of Tada, et al. and SINTAP are described in Sections A1 and A2, respectively. The results are shown in Section A3.

A1 Tada, Paris, and Irwin Solution [12]

By Linear Elastic Fracture Mechanics (LEFM), the opening mode (Mode I) stress intensity factor (K_I) of a crack in the cladding longitudinal (axial) direction is

$$K_I = \sigma\sqrt{\pi c}\cdot F(\rho)$$

where c is the half crack length, σ is the tensile stress to open the crack ($\sigma = \sigma_h$ in the present case), $\rho = c/\sqrt{Rt}$, t is the cladding thickness, and the geometric-dependent function $F(\rho)$ is

$$F(\rho) = \sqrt{1 + 1.25\rho^2} \qquad \text{for } 0 < \rho \le 1$$

$$F(\rho) = 0.6 + 0.9\rho \qquad \text{for } 1 \le \rho \le 5$$

The companion solution for the crack opening area (COA) and the geometry-dependent function $G(\rho)$ are

$$COA = \frac{\sigma}{E}2\pi Rt\cdot G(\rho)$$

$$G(\rho) = \lambda\rho^2 + 0.625\rho^4 \qquad \text{for } 0 < \rho \le 1$$

* Strictly speaking, Eq. (8) is only applied to the inner most element of the cladding where the press-fit pressure (p) is acting. Eq. (8) could be overly conservative to apply to the majority of the cladding.

$$G(\rho) = 0.14 + 0.36\lambda\rho^2 + 0.72\rho^3 + 0.405\rho^4 \qquad \text{for } 1 \le \rho \le 5$$

A2 SINTAP Solution

The stress intensity factor formula proposed by the Structural INTegrity Assessment Procedures (SINTAP) for European Industry [14] is similar to that reported by Tada, et al. (Section A1). However, SINTAP equations are given for both crack tips - on the internal surface (K_{in}) and on the external surface (K_{out}), as depicted in Figure 4. In the case of no bending stress, the stress intensity factor solutions are written as

$$K_{in} = \sigma\sqrt{\pi c}\,(G1(\rho) - g1(\rho))$$

$$K_{out} = \sigma\sqrt{\pi c}\,\big(G1(\rho) + g1(\rho)\big)$$

where

$$\rho = c/\sqrt{Rt}$$

$$G1(\rho) = \sqrt{1 + 0.7044\rho + 0.8378\rho^2}$$

and

$$g1(\rho) = -0.035211 + 0.39394\rho - 0.20036\rho^2 + 0.028085\rho^3 - 0.0018763\rho^4 + \frac{\left(3.912 - \ln\left(\frac{R}{t}\right)\right)}{1.6094}(0.01556 - 0.05202\rho + 0.0381\rho^2 - 0.012782\rho^3 + 0.001246\rho^4)$$

The range of Applicability is $0 \le \rho \le 4.4$.

Without considering the crack face plasticity effect, the crack opening area, *COA*, is expressed as [14, 16, 17]

$$COA = \Upsilon(\omega)\frac{2\pi c^2\sigma}{E}$$

$$\Upsilon(\omega) = 1 + 0.1\omega + 0.16\omega^2$$

$$\omega^4 = 12(1 - \upsilon^2)\frac{c^4}{R^2t^2}$$

These equations are also adopted by British Standard (BS-7910 [15]).

A3 Comparison of Critical Crack Length and Crack Opening Area from Various Formulations

Given two bounding fracture toughness values (K_{IC} = 25 and 90 MPa√m), the critical crack lengths were calculated for given hoop strains (which are proportional to the hoop stresses) by Tada et al. (Section A1), SINTAP (Section A2), and API 579 (Section 3.1 [9]). The results are shown in Figure A1. Similarly, the crack opening areas were obtained and shown in Figure A2. It can be seen that the API 579 approach

consistently gives more conservative results. That is, for a given cladding hoop stress or strain, API 579 predicts lowest values for critical crack length and crack opening area. Therefore, API 579 was chosen for the full fracture analysis in Section 3 of the report. However, the results also show that SINTAP solutions for both critical crack length and opening area are very close to those determined with API 579 procedure, at least for the present calculation range. Therefore, if a quick assessment is needed, the SINTAP formulation (Section A2) may be considered. Note that some SINTAP procedures are consistent with the British Standards (BS-7910 [13-16]). On the other hand, the equations provided by Tada et al. [12] are the easiest to use (Sections A1), but might contain small but sometimes acceptable errors due to simplification.

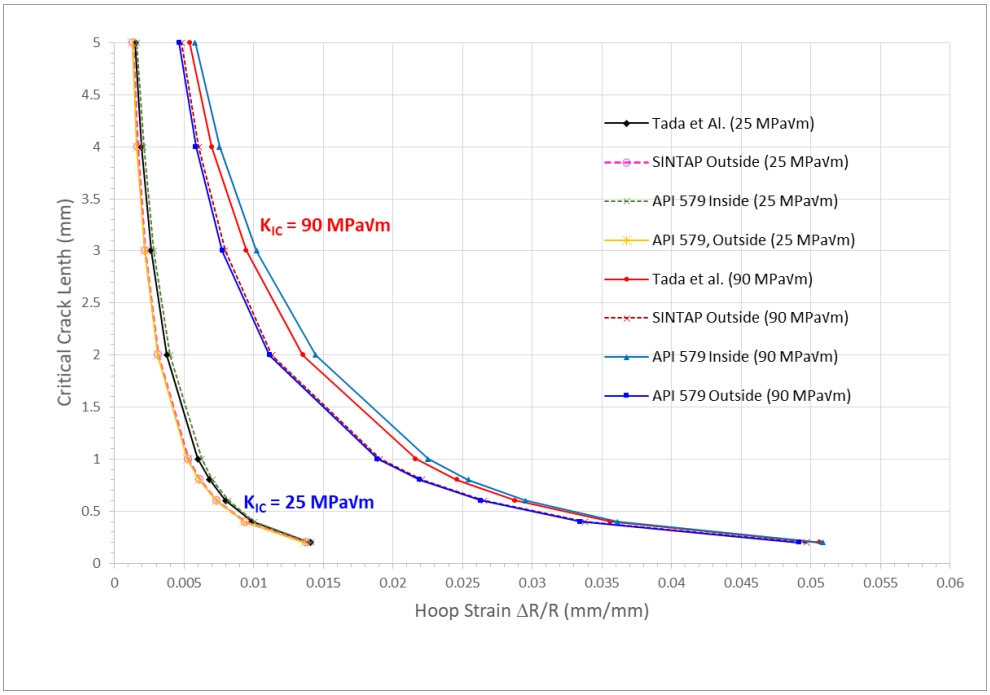

Figure A-1. Comparison of critical crack lengths calculated by Tada, et al. [12], SINTAP [14], and API 579 [9]

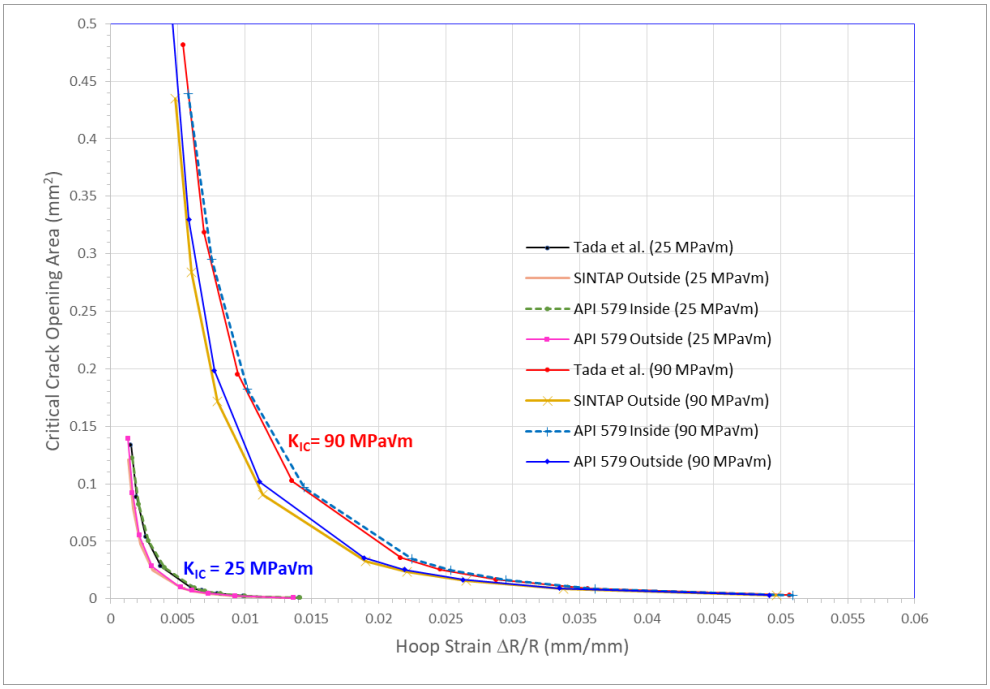

Figure A-2. Comparison of critical crack opening areas calculated by Tada, et al. [12], SINTAP [14], and API 579 [9]